GAVIN PUBLISHERS

Ophthalmology Research & Reports

Bringmann A, et al. Ophthalmol Res Rep 6: 151.

Research Article

DOI: 10.29011/2689-7407.100051

Two Types of Curved Hyperreflective Structures on Optical Coherence Tomography Images of the Outer Retina of Eyes with Different Macular Disorders

Andreas Bringmann, Jan Darius Unterlauft, Thomas Barth, Renate Wiedemann, Matus Rehak, Peter Wiedemann*

Department of Ophthalmology and Eye Hospital, University of Leipzig, Leipzig, Germany

***Corresponding author:** Peter Wiedemann, Department of Ophthalmology and Eye Hospital, University of Leipzig, Leipzig, Germany

Citation: Bringmann A, Unterlauft JD, Barth T, Wiedemann R, Rehak M, et al. (2021) Two Types of Curved Hyperreflective Structures on Optical Coherence Tomography Images of the Outer Retina of Eyes with Different Macular Disorders. Ophthalmol Res Rep 6: 151. DOI: 10.29011/2689-7407.100051

Received Date: 12 August, 2021; **Accepted Date:** 23 August, 2021; **Published Date:** 27 August, 2021

Abstract

Hyperreflective materials on Spectral-Domain Optical Coherence Tomography (SD-OCT) images of eyes with different retinal disorders may have diverse shapes and origins and are a prognostic marker of disease progression. This study documents using SD-OCT the presence of Curved Hyper Reflective Structures (CHRS) in the outer macula of eyes with different retinal disorders. A retrospective case series of 22 eyes of 21 patients with CHRS is described. In addition, 12 eyes of 12 patients with other kinds of intra retinal hyperreflective structures were investigated. CHRS, which form curved thin lines or broad bands between the outer plexiform layer and external limiting membrane (ELM) in the macula, were found in eyes without edema. Thin CHRS were secondary to dry age-related macular degeneration (AMD; n=10 eyes), glaucoma (n=2), wet AMD, chorioretinitis, macular scarring, anterior ischemic optic neuropathy, proliferative diabetic retinopathy, adult-onset foveomacular vitelliform dystrophy, and ocular ischemia (each n=1), respectively. Broad CHRS were caused by hemorrhages in the inner foveal layers (n=3). CHRS were associated with focal photoreceptor layer defects. The defects were present before the formation of thin CHRS and during or after the formation of broad CHRS. The retina of eyes with edema showed hyper reflective foci and cystoid cavities which contained hypo- or medium-reflective fluid and hyper reflective material, but not CHRS. It is concluded that CHRS in the outer macula are found in eyes with different retinal disorders without edema. Thin CHRS likely develop after photoreceptor damage from the ELM. Broad CHRS are caused by hemorrhages within the inner foveal layers.

Keywords: Age-related macular degeneration; Cystoid macular edema; Drusen; Exudate; Hyperreflective foci; Intraretinal hemorrhage

Abbreviations: AION: Anterior Ischemic Optic Neuropathy; AMD: Age-Related Macular Degeneration; AOFVD: Adult-Onset Foveomacular Vitelliform Dystrophy; BCVA: Best-Corrected Visual Acuity; BRVO: Branch Retinal Vein Occlusion; CHRS: Curved Hyperreflective Structure; CME: Cystoid Macular Edema; CNV: Choroidal Neovascularization; DME: Diabetic Macular Edema; ELM: External Limiting Membrane; EZ: Ellipsoid Zone; GCL: Ganglion Cell Layer; HFL: Henle Fiber Layer; INL: Inner Nuclear Layer; IPL: Inner Plexiform Layer; IZ: Interdigitation Zone; NFL: Nerve Fiber Layer; ONL: Outer Nuclear Layer; OPL: Outer Plexiform Layer; PDR: Proliferative Diabetic Retinopathy; RPE: Retinal Pigment Epithelium; SD-OCT: Spectral-Domain Optical Coherence Tomography

Introduction

Intraretinal deposits of hyperreflective material, which may display diverse shapes like dots, spots, and patches on Spectral-Domain Optical Coherence Tomographic (SD-OCT) images, is a characteristic of different retinal diseases. Hyperreflective foci are found on SD-OCT images of eyes with dry or wet Age-Related Macular Degeneration (AMD), acquired vitelliform lesions, central serous chorioretinopathy, Diabetic Macular Edema (DME), and other vascular and inflammatory diseases like retinal vein occlusion and uveitis [1-7]. In patients with intermediate AMD, intraretinal accumulation of hyperreflective foci is an important risk factor for the progression to late AMD, in particular for the development of geographic atrophy characterized by the degeneration of the

Retinal Pigment Epithelium (RPE) and photoreceptors [8-10]. The quantity of intraretinal hyperreflective foci is also a predictor for the visual outcome in other retinal disorders like central serous chorioretinopathy and diabetic retinopathy [11-14].

In eyes of patients with wet AMD, hyperreflective foci are scattered throughout the retinal tissue but are mainly located in the outer layers around fluid accumulations [15]. Hyperreflective material in the outer neuroretina of AMD eyes is often attached to the apex of drusen or drusenoid RPE detachments; the presence of hyperreflective structures above drusen is associated with a thinning of the photoreceptor and outer retinal layers and an increased risk of local atrophy [16-21]. In eyes of diabetic patients, hyperreflective material is primarily deposited in the Henle Fiber Layer (HFL) [22-25]; smaller hyperreflective foci can be found in all retinal layers [2,26]. Confluence of hyperreflective foci to larger plaques in the HFL is visible on fundus photographs as hard exudate [2,3,25,27]. The pathogenesis of intraretinal hyperreflective deposits is incompletely understood. Depending on the type of retinal disease and the size, shape, and location of the deposits, lipoprotein exudation, microglia activation, macrophage recruitment, and RPE cell migration were suggested as possible causes [1-4,6,17,22,23,28-33].

In the present study, we describe the occurrence of hyperreflective material of conspicuous shape in eyes with various retinal disorders. The hyperreflective material forms curved structures in the outer macular layers and is visible on SD-OCT images as thin lines or broad bands between the Outer Plexiform Layer (OPL) and External Limiting Membrane (ELM). In AMD eyes, these Curved Hyperreflective Structures (CHRS) have been referred to as a plume [21]. A further aim of the present study was to compare the intraretinal distribution of hyperreflective material in eyes without and with Cystoid Macular Edema (CME).

Methods

This is a retrospective, single-center chart review. The study followed the ethical standards of the 1964 Declaration of Helsinki and its later amendments. The protocol was approved by the Ethics Committee of the Medical Faculty of the University of Leipzig (#143/20-ek). The ethics committee is registered as Institutional Review Board at the Office for Human Research Protections (registration number, IORG0001320/IRB00001750). The patients gave their informed consent for their images and other clinical information to be reported. We retrospectively reviewed the charts of 89,317 patients who were referred to the Department of Ophthalmology, University of Leipzig, Germany, between August 2008 and December 2019. We searched for charts which contained SD-OCT images that showed the presence of CHRS in the outer macula. We found charts of 22 eyes of 21 patients which fulfilled this criterion. We also included 12 eyes of 11 patients which exhibited intraretinal hyperreflective material of other shapes. Table 1 summarizes the patient's characteristics. All patients were Caucasians. Exclusion criteria were presence of an intraocular tumor, high myopia (>6 diopters), and poor quality of OCT imaging. In addition, we included SD-OCT images of 4 eyes of 4 subjects without apparent eye disease in which the HFL was distinguishable from the Outer Nuclear Layer (ONL) (3 women, 1 man; mean age, 60.8±8.9 years; range 45-72 years).

Figure (Image)	**Sex**	**Age** (years)	**BCVA**	**Aetiology**
1A (1)	w	81	0.5	dry AMD
1A (2)	w	63	0.63	dry AMD
1A (3)	m	76	0.8	dry AMD, RPE scarring without CNV
1A (4)	m	69	0.8	dry AMD
1A (5)	w	79	0.6	dry AMD
1A (6)	w	81	0.5	dry AMD
1A (7)	w	77	0.63	dry AMD
1A (8)	m	61	1.0	dry AMD, RPE scarring without CNV
1A (9)	w	48	1.0	chorioretinitis
1A (10)	m	49	0.1	macular scarring
1A (11, 12)	m	74	1.0 / 0.8	AION resulting from arteria carotis interna stenosis
1A (13)	w	79	0.8	PDR, intravitreal ranibizumab (Lucentis)
1A (14)	w	75	0.2	glaucoma
1A (15)	m	64	0.8	glaucoma

2A	w	51	0.2 to 0.4	CNV, intravitreal ranibizumab (Lucentis)
2B	m	66	0.63 to 0.63	ocular ischemia syndrome
2C	w	69	0.8 to 0.6	AOFVD
2D	w	51	0.5	AOFVD
2E	m	81	0.5 to 0.5	dry AMD
2F	m	63	0.8 to 0.8	intraretinal hemorrhage
2G	m	60	0.8	intraretinal hemorrhage
2H	m	77	0.63	intraretinal hemorrhage
2I	m	42	0.8 to 1.0	Valsalva retinopathy
3A	w	68	1.0	BRVO
3B	m	59	1.0 to 1.0	macroaneurysm, intravitreal triamcinolone
3C	w	66	0.4	hypertensive retinopathy
3D	w	69	0.8 to 1.0	NPDR, macular edema
3E	m	59	0.4 to 0.5	NPDR, macular edema, intravitreal ranibizumab (Lucentis)
3F	m	64	0.5 to 0.4	NPDR, macular edema
3G	m	61	0.5 to 0.63	BRVO, macular edema
3H	w	77	0.50 to 0.25	BRVO, macular edema, intravitreal ranibizumab (Lucentis)
3I	w	47	1.0	central serous chorioretinopathy

AOFVD: Adult-Onset Foveomacular Vitelliform Dystrophy; AION: Anterior Ischemic Optic Neuropathy; AMD: Age-Related Macular Degeneration; BRVO: Branch Retinal Vein Occlusion; CNV: Choroidal Neovascularization; m: Man; NPDR: Nonproliferative Diabetic Retinopathy; PDR: Proliferative Diabetic Retinopathy; PVD: Posterior Vitreous Detachment; w: Woman

Table 1: Patients' characteristics. Best-Corrected Visual Acuity (BCVA) is given for the first visit and the end of the examination period where appropriate.

5.5-mm, 6-line radial scans of the macula were recorded with SD-OCT (Spectralis, Heidelberg Engineering, and Heidelberg, Germany). Fundus images were obtained using a Nidek AFC-230 camera (Nidek Co., Ltd., Aichi, Japan). Best-corrected visual acuity (BCVA) was determined using Snellen charts and is given in decimal units.

Distances on SD-OCT images were measured using Heyex 2 (Heidelberg Engineering). The horizontal extension of CHRS was measured between the OPL and ELM; the distance to the foveal center was measured between the ELM and the tip of the fovea externa (Figure 1B). Data are given as means ± S.D. Statistical analysis was performed using Prism (Graphpad Software, San Diego, CA). Significant differences were evaluated with the non-parametric Mann-Whitney U test, and were accepted at $P<0.05$.

Results

CHRS in the outer macula

Figure 1A shows SD-OCT images of the macula of 15 eyes of 14 patients which displayed CHRS between the OPL and ELM. The patients suffered from different retinal diseases including dry AMD (images 1-8), chorioretinitis, macular scarring, Anterior Ischemic Optic Neuropathy (AION), proliferative diabetic retinopathy (PDR), and glaucoma (Table 1). In four eyes, CHRS passed through the ONL and HFL, but did not reach the OPL (images 5, 10, 11, 15). The thickness of CHRS varied in the eyes. Thin CHRS were composed of discrete hyperreflective dots ordered in linear shape (images 2, 5, 14) while thicker CHRS were composed of adjoining dots (e.g., images 1 and 15). In different eyes, single hyperreflective dots had a diameter between 21 and 39 µm; the

mean diameter was 31.0 ± 7.0 µm (n=31 dots). In all eyes investigated, CHRS were associated with a focal loss of photoreceptor integrity, as indicated by irregular reflectivity, deformation, and/or disruption of the Ellipsoid Zone (EZ) and the Interdigitation Zone (IZ) lines.

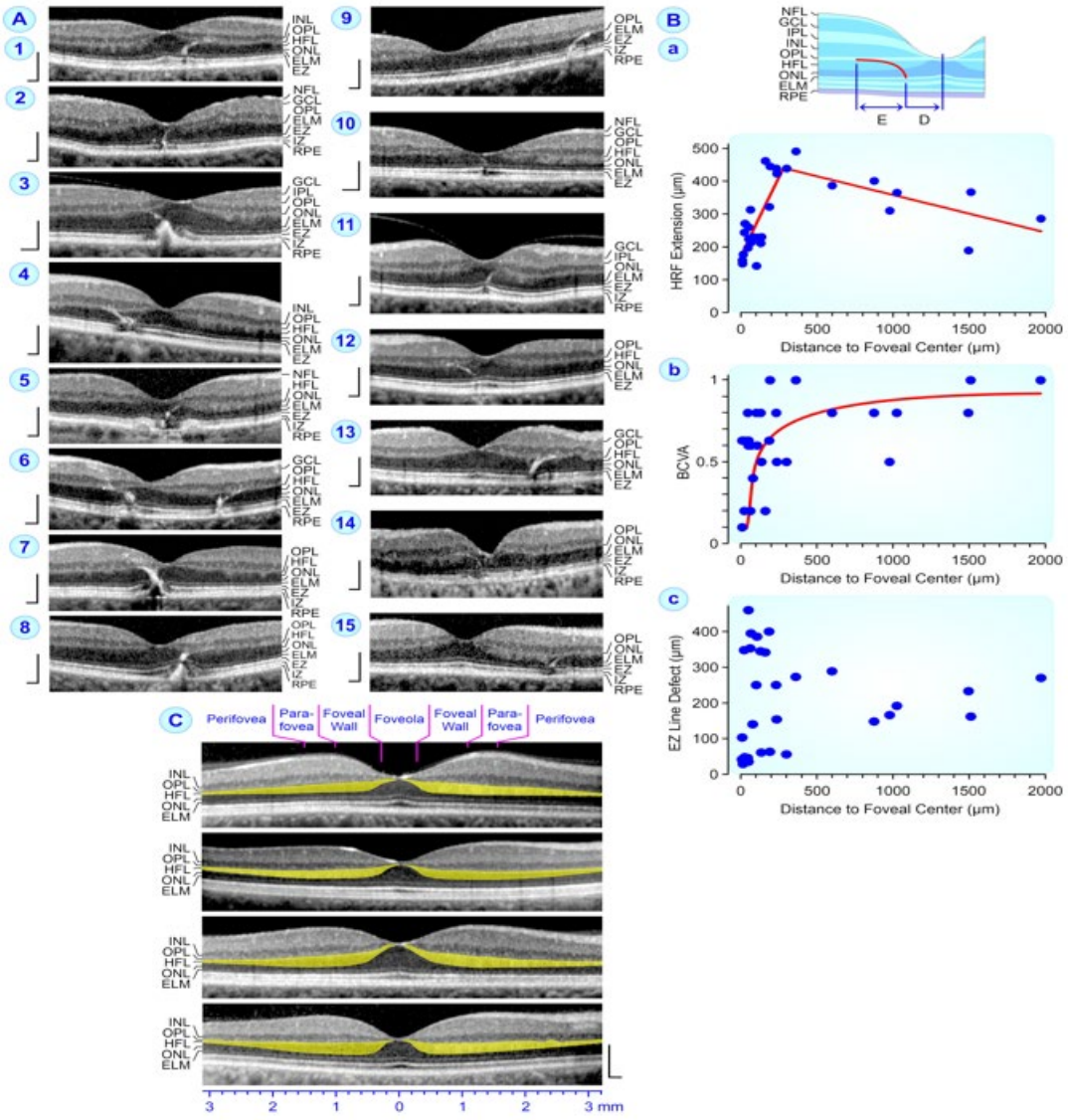

Figure 1: Curved Hyperreflective Structures (CHRS) between the Outer Plexiform Layer (OPL) and External Limiting Membrane (ELM) are associated with focal loss of photoreceptor integrity. **A**. SD-OCT images of the foveas and parafoveas of 15 eyes of 14 patients with CHRS in the Henle Fiber Layer (HFL) and Outer Nuclear Layer (ONL). **B**. Parameters of CHRS measured on SD-OCT images of 20 eyes. **a**. Scatter plot of the relation between the horizontal extension (E) and the distance (D) of CHRS to the foveal center. **b**. Relation between the Best-Corrected Visual Acuity (BCVA) of the eyes and the distance (D) of CHRS to the foveal center. **c**. Relation between the widths of the Ellipsoid Zone (EZ) line defect associated with CHRS and the distance (D) of the CHRS to the foveal center. **C**. Linear horizontal SD-OCT scans through the macula of four human subjects without apparent eye disease. The HFL is shown in yellow. The temporal macula is shown at the left side, the nasal macula at the right side. Scale bars, 200 µm. GCL: Ganglion Cell Layer; INL: Inner Nuclear Layer; IPL: Inner Plexiform Layer; IZ: Interdigitation Zone; NFL: Nerve Fiber Layer; RPE: Retinal Pigment Epithelium.

Five eyes (images 3, 6-9) displayed drusenoid RPE detachments from Bruch's membrane; the RPE formed excrescences which protruded towards or into the outer neuroretina. In two eyes (images 3, 8), the protrusions caused a compression of the outer retina including the photoreceptors resulting in a thinning of the HFL and ONL. In three eyes, CHRS were connected to the RPE (images 6, 7, 9).

The shape of CHRS in the outer macula apparently followed the spatial arrangement of the Henle fibers in the HFL and the rows of photoreceptor cell bodies in the ONL. To prove this assumption, we measured two parameters of CHRS in SD-OCT images of 20 eyes: the horizontal extension and the distance to the foveal center (Figure 1Ba). Figure 1Ba shows the horizontal extension of CHRS in dependence to the distance to the foveal center. The horizontal extension increased continuously from the foveal center up to about 300 µm and declined with a smaller slope at distances greater than 400 µm from the foveal center (Figure 1Ba). Normally, the HFL has the same low reflectivity as the ONL; therefore, the HFL and ONL are usually not distinguishable in SD-OCT images (Figure 1A). However, the reflectivity of the HFL depends on the angle at which the light hits the retina [34,35]. Figure 1C shows SD-OCT images of eyes of human subjects without apparent eye disease in which the HFL was distinguishable from the ONL. The peak thickness of the HFL was between 300 and 500 µm from the foveal center, i.e., in the foveal walls surrounding the foveola. This value is similar to that of the largest horizontal extension of CHRS and supports the assumption that the shape of CHRS follows the spatial arrangement of the Henle fibers in the HFL.

Figure 1Bb shows the relation between BCVA of eyes with CHRS and the distance of CHRS to the foveal center. The BCVA of eyes with CHRS in the foveola (i.e., within a distance of 300 µm from the foveal center; (Figure 1C) varied considerably (Figure 1Bb). Although the mean BCVA of eyes with CHRS within a distance of 300 µm to the foveal center was smaller (0.58±0.23; n= 15) than that of eyes with CHRS outside the foveola (0.78±0.18; n=5), this difference was not significant ($P>0.05$).

Defects of EZ and IZ lines reflect deconstruction of photoreceptor segments. Figure 1Bc shows the relation between the width of the CHRS-associated EZ line defect and the distance of the CHRS to the foveal center. In different eyes, the width of the EZ line defect varied considerably within the foveola. There were no correlations between the BCVA and the distance of CHRS to the foveal center and the width of the EZ line defect, respectively (data not shown).

Formation and morphological alterations of hyperreflective structures in the fovea. Figures 2A-2C shows examples of early stages of CHRS formation in the outer fovea. The SD-OCT scans of Figure 2A were recorded in an eye with Choroidal Neovascularization (CNV) that was treated with intravitreal ranibizumab (Lucentis). CHRS formed after a transient serous detachment of the fovea from the RPE (first visit). After reattachment of the fovea, the outer fovea contained irregularly shaped clumps of hyperreflective material near the ELM (1 month). The photoreceptor layer between the ELM and RPE was also hyperreflective. Thereafter, a CHRS was formed which was connected to a clump of the hyperreflective material (2.2 months).

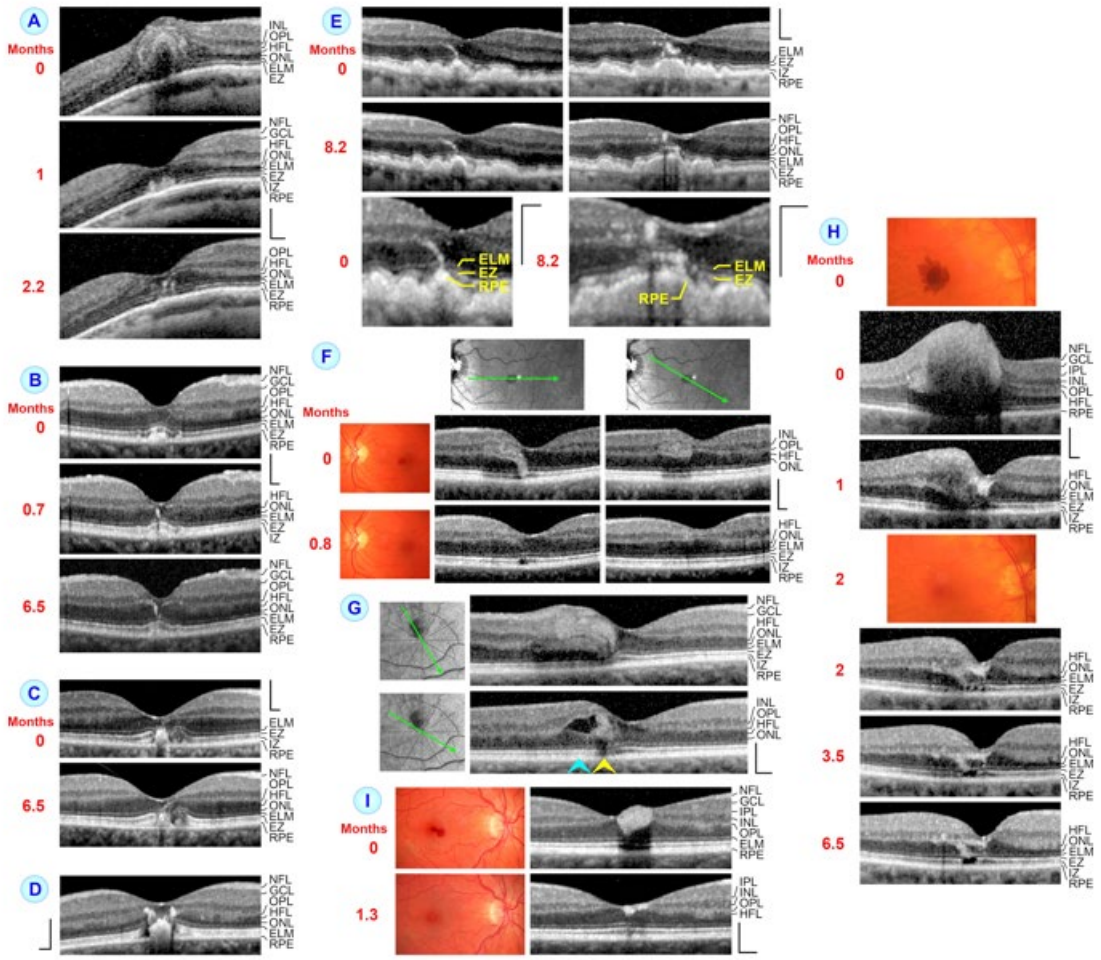

Figure 2: Formation and time-dependent alterations of hyperreflective structures in the fovea. The images show SD-OCT scans through the foveas and parafoveas of 10 eyes of 9 patients. The months after the first visit (0) are indicated left of the images. **A–C**. Formation of Curved Hyperreflective Structures (CHRS) in the central outer fovea in eyes with choroidal neovascularization **(A),** ocular ischemia syndrome **(B),** and adult-onset foveomacular vitelliform dystrophy **(C),** respectively. **D**. Another eye with adult-onset foveomacular vitelliform dystrophy. **E**. CHRS in the outer macula of the left eye (left side) of a patient with dry age-related macular degeneration. The right side shows scans from the right eye. Note that the hyperreflective structures in the outer macula of both eyes were in front of large drusen and that the hyperreflective structures in the Outer Nuclear Layer (ONL) were connected to the material in the photoreceptor layer. The images below show parts of the scans recorded in the left and right eyes at higher magnification. **F.** Partial reabsorption of a broad CHRS associated with hemorrhage in the Inner Nuclear Layer (INL). CHRS extended between the INL and the Ellipsoid Zone (EZ). The orientations of the scans are shown above the images. **G**. An eye with a hemorrhage between the Ganglion Cell Layer (GCL) and INL of the nasosuperior foveal wall and parafovea. The upper image shows a broad CHRS within the Henle Fiber Layer (HFL) and ONL. The lower image shows a cystoid cavity between the Outer Plexiform Layer (OPL) and HFL which is filled by hyporeflective fluid (blue arrowhead) and a large patch of hyperreflective material (yellow arrowhead). **H**. The reabsorption of a hemorrhage in the inner foveal layers of this eye was associated with the formation of a broad CHRS and a degeneration of photoreceptors. **I**. SD-OCT (right) and fundus images (left) of an eye with Valsalva retinopathy. After resolution of the intraretinal hemorrhage, hyperreflective deposits were present in the inner layer of the foveola. Scale bars, 200 µm. ELM: External Limiting Membrane; IPL: Inner Plexiform Layer; IZ: Interdigitation Zone; NFL: Nerve Fiber Layer; RPE: Retinal Pigment Epithelium.

Figure 2B shows scans recorded in an eye with ocular ischemia syndrome in which two CHRS developed in the central fovea. The RPE of the foveola was thickened; this was associated with an anterior displacement of the ELM, EZ, and IZ lines. The scans shown in Figure 2C were recorded in an eye with Adult-Onset Foveomacular Vitelliform Dystrophy (AOFVD). There was a broad area with defects of the ELM, EZ, and IZ lines in the central fovea; in this area, the hyperreflective material in the subretinal space protruded towards the foveal neuroretina. The reflectivity of two CHRS increased within 6.5 months after the first visit; both CHRS were connected to the hyperreflective subretinal material. Figure 2D shows a scan obtained in another eye with AOFVD. The HFL and ONL above the area with broad defects of the ELM, EZ, and IZ lines contained large irregularly formed clumps of hyperreflective material. The subretinal space comprised hyperreflective material which partly represented the RPE that was detached from Bruch's membrane. The hyperreflective deposits in the ONL and HFL of the fovea extended at various sites into the subretinal space.

Figure 2E shows SD-OCT scans recorded in both eyes of a patient with dry AMD. The scans of the left eye display a CHRS in the HFL and ONL while the scans of the right eye show irregularly arranged hyperreflective material in the HFL and ONL of the fovea. In both eyes, the hyperreflective structures in the outer neuroretina were located in front of large drusen and were connected to the RPE. In the right eye, a hyperreflective patch developed in the Inner Nuclear Layer (INL) after the partial regression of the hyperreflective material in the HFL.

Figure 2F–H shows SD-OCT scans recorded in eyes with hemorrhage in the inner foveal layers. The scans of Figure 2F show a hemorrhage within the INL of the nasal foveal wall and parafovea. The hemorrhage was associated with an expansion of the INL and displacements of the inner part of this layer and of the OPL; hyperreflective material accumulated in the mid and outer part of the INL, suggesting that the origin of the bleeding was a defect of the deep capillaries at the outer border of the INL. The displacements of the inner part of the INL and OPL caused compression of the Inner Plexiform Layer (IPL) and the outer retina. The hyperreflective material in the INL merged with a broad CHRS which reached up to the EZ line. There were outward deflections of the ELM and EZ lines and a defect of the IZ line below the CHRS. The hemorrhage regressed within few weeks after the first examination; this was associated with a nearly full disappearance of the CHRS. A focal photoreceptor defect remained, as indicated by the hyporeflectivity of the EZ line and the defect of the IZ line.

The scans of Figure 2G show a hemorrhage between the Ganglion Cell Layer (GCL) and INL which caused a thickening of the foveal wall and parafovea. The hemorrhage merged with broad CHRS in the HFL and ONL of the more superior fovea as well as with a hyperreflective deposit within the cystoid cavity between the OPL and HFL in the more inferior fovea. The outward deflection of the ELM and the defects of the EZ and IZ lines indicate a loss of photoreceptor integrity below the broad CHRS. The scans of Figure 2H show the formation of a broad CHRS associated with a deconstruction of photoreceptor segments after reabsorption of a hemorrhage in the inner foveal layers. The presence of hyperreflective material in the GCL and OPL of the parafovea one month after the first visit may suggest that hemorrhage resulted from bleeding from both superficial and deep vascular plexus. The hemorrhage was associated with a pressure onto the outer neuroretina as indicated by the outward deflections of the RPE line at the first visit and of the ELM line one month later. The defects of the EZ and IZ lines below the outwardly deflected ELM line suggests that the pressure was associated with a deconstruction of photoreceptor segments. After reabsorption of the hemorrhage in the inner foveal layers, there remained a broad CHRS and hyperreflective material in the HFL of the foveal wall and the stalk of the Müller cell cone in the foveola. The EZ and IZ lines restored around the photoreceptor-free area below the CHRS.

The scan of an eye with Valsalva retinopathy (Figure 2I) recorded at the first examination shows an intraretinal hemorrhage in the nasal part of the central fovea. After resolution of the hemorrhage, hyperreflective material accumulated in the inner layer of the foveola; the shape of the hyperreflective deposit resembled that of the Müller cell cone [36].

Hyperreflective structures in eyes with different diseases. CHRS were found in eyes without retinal edema. Intraretinal hyperreflective structures with different shape like foci, dots, and patches were described to be a characteristic of various retinal diseases including AMD and DME [2,4,24]. In order to investigate whether retinal disorders with edema may be associated with formation of CHRS, we included SD-OCT scans of 9 eyes of 9 patients which showed intraretinal deposits of hyperreflective material. None of these eyes showed a curved arrangement of hyperreflective material in the outer macula.

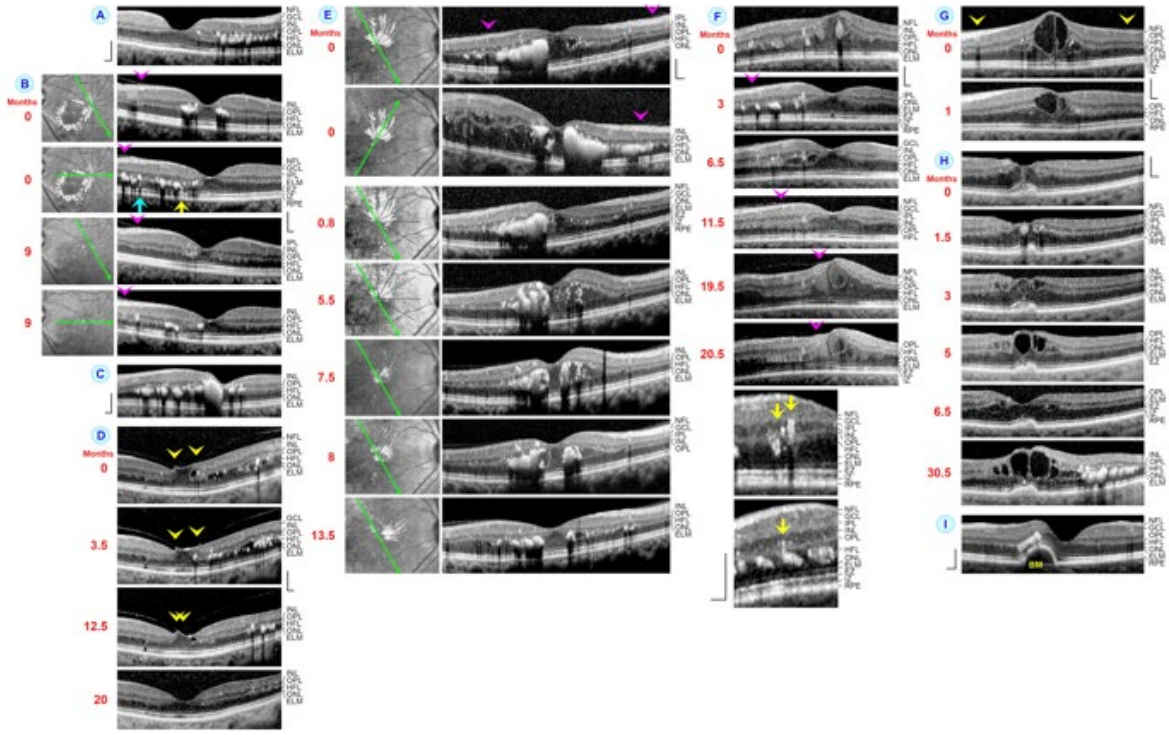

Figure 3: Hyperreflective material in eyes with different retinal diseases. The images show SD-OCT scans through the foveas and parafoveas of 9 eyes of 9 patients. The months after the first visit (0) are indicated left of the images. The arrowheads indicate adhesions of the partially detached posterior hyaloid at the macular tissue. In **B** and **E**, the orientations of the scans are shown at the left side. **A**. An eye with Branch Retinal Vein Occlusion (BRVO). Hyperreflective material was located in the Inner Nuclear Layer (INL), Outer Plexiform Layer (OPL), and Henle Fiber Layer (HFL) of the foveal wall, para-, and perifovea at the right side. **B**. Partial reabsorption of hyperreflective patches in the INL, OPL, HFL, and Outer Nuclear Layer (ONL) of the macula in an eye with macroaneurysm. The initial fundus scan (left) shows a ring of hyperreflective material in the nasoinferior macula. The yellow arrow indicates a connection between hyperreflective materials in the ONL and in the subretinal space. The blue arrow indicates hyperreflective material which passed through the External Limiting Membrane (ELM). **C**. An eye with hypertensive retinopathy and cystoid spaces in the HFL which were filled with hyporeflective fluid and hyperreflective material. **D**. An eye with Nonproliferative Diabetic Retinopathy (NPDR) associated with macular edema. Hyporeflective cystoid spaces in the HFL contained clumps of hyperreflective material. Hyaloidal traction deformed the foveal shape. The detachment of the posterior hyaloid from the fovea (after 3.5 months) was followed by the resolution of the cystoid cavities and reabsorption of the hyperreflective deposits. **E**. Another eye with NPDR and Cystoid Macular Edema (CME). The cystoid spaces in the HFL were filled with medium-reflective fluid and hyperreflective material. The size of the cystoid spaces varied during the examination period; this was associated with a varying thickness of the foveal tissue. The fundus scans (left) show a partial star of hard exudates. **F**. A further eye with NPDR and CME. The cystoid spaces in the HFL were filled with medium-reflective fluid and hyperreflective material. Smaller hyperreflective foci were also present at some sites within the INL, Inner Plexiform Layer (IPL), and Ganglion Cell Layer (GCL). The smaller images below show parts of the scans recorded 3 months after the first visit at higher magnification. The arrows indicate patches composed of adjoining hyperreflective dots (above) and hyperreflective material in the INL and OPL was continuous to the material in the HFL. **G**. An eye with BRVO and CME. There were large cystoid cavities in the foveola and cystoid spaces between the OPL and HFL of the foveal walls. Small hyperreflective foci were present in the INL, OPL, and HFL. **H**. Another eye with BRVO and CME. **I**. An eye with central serous chorioretinopathy associated with a dome-shaped detachment of the Retinal Pigment Epithelium (RPE) from the Bruch's Membrane (BM). Scale bars, 200 µm. EZ: Ellipsoid Zone; IZ: Interdigitation Zone; NFL: Nerve Fiber Layer.

Figure 3A shows an SD-OCT image which was recorded in an eye with Branch Retinal Vein Occlusion (BRVO) without CME, a condition which was recently described as "HFL hemorrhage" [37]. Clumps of hyperreflective material were present in the INL, OPL, and HFL; at many sites, the material in the INL was connected to that in the OPL and HFL. The scans of Figure 3B were obtained in an eye with macroaneurysm that was treated with intravitreal injection of triamcinolone acetonide. The fundus scan recorded at the first visit shows a ring of hyperreflective material in the nasoinferior macula. Patches of hyperreflective material were present in the INL, OPL, HFL, and ONL of the foveal walls, para-, and perifovea. At many sites, the hyperreflective material formed continuous structures between the INL and ONL. At one site, the hyperreflective material in the OPL was continuous with the material in the subretinal space (yellow arrow in Figure 3B). At another site, hyperreflective material passed through the ELM (blue arrow). The intraretinal hyperreflective material was partially absorbed within 9 months after the first visit. The large hyperreflective clumps in the foveal walls became smaller hyperreflective foci scattered between the GCL and HFL.

The SD-OCT image of Figure 3C was recorded in an eye with hypertensive retinopathy. The intraretinal distribution of hyperreflective material was similar to that of the eyes shown in Figure 3A and B. In addition, there were hyporeflective cystoid spaces in the HFL between the patches of the hyperreflective material, indicating CME. At various sites, the hyperreflective material in the INL was connected with that in the cystoid spaces of the HFL.

Figure 3D-3F shows SD-OCT scans recorded in eyes with nonproliferative diabetic retinopathy and CME. The CME of the eye shown in Figure 3D was characterized by cystoid spaces in the HFL which were filled by hyporeflective fluid and clumps of hyperreflective material; smaller hyperreflective foci were present in the IPL, INL, and OPL. Hyaloidal traction deformed the foveal shape. During the examination period, the posterior hyaloid fully detached from the fovea. The detachment was followed by a resolution of the cystoid spaces and a nearly full reabsorption of the hyperreflective material.

The eye of Figure 3E was treated with intravitreal ranibizumab (Lucentis). The fundus images (left side of Figure 3E) show a partial macular star configuration caused by light reflection at large accumulations of hyperreflective material in the edematous cystoid spaces within the HFL; smaller hyperreflective foci in the HFL, INL, IPL, and GCL did not contribute to the hyperreflective stellate figure in the fundus scans. At 5.5 months after the first visit, there were also large accumulations of hyperreflective material in the GCL, IPL, and INL which merged with the material in the HFL. The large hyperreflective patches in the GCL, IPL, and INL regressed until the end of the examination period. The cystoid spaces in the HFL contained medium-reflective fluid and varying amounts of hyperreflective foci and patches. Enlargement of the edematous cystoid spaces was associated with an elevation of the inner foveal layers (Nerve Fiber Layer [NFL] to OPL) which caused a thickening of the macular tissue.

The CME of the eye shown in Figure 3F was characterized by cystoid spaces in the HFL which were filled with medium-reflective fluid and patches of hyperreflective material. Smaller hyperreflective foci were also present in the inner foveal layers. Resolution of the cystoid cavities was followed by a nearly complete reabsorption of the hyperreflective material (11.5 months). Redevelopment of the CME was again associated with the formation of cystoid spaces filled with medium-reflective fluid and smaller hyperreflective foci; the walls of a large central cystoid cavity were lined by hyperreflective dots (19.5 months). Larger hyperreflective patches were composed of adjoining dots; single dots had a mean diameter of 38.5 µm (range, 33–48 µm). At one site, hyperreflective material in the outer part of the INL and OPL continued to the material in the HFL.

Figure 3G and H show SD-OCT scans recorded in two eyes with BRVO and CME. The foveola of the eye shown in Figure 3G contained a large cystoid cavity. The hydrostatic pressure within the cavity caused a detachment of the inner Müller cell layer from the HFL/ONL which was associated with an anterior stretching and elongation of the stalk of the Müller cell cone. The detachment of the inner Müller cell layer of the foveola was combined with an elevation of the inner layers of the foveal walls (NFL to OPL) and a schisis between the OPL and HFL of the foveal walls. The schistic cavities were filled with medium-reflective fluid; there were few hyperreflective dots at various sites in the cavities and the INL.

The scans of Figure 3H were recorded in an eye with BRVO and drusen below the foveola; the eye was treated with intravitreal ranibizumab (Lucentis). At 1.5 months after the first examination, the inner tissue of the foveola contained a hyperreflective structure which might be formed from the medium-reflective material which drew through the center of the foveola at the first visit. Thereafter, an edematous cystoid cavity developed in the foveola, which contained medium-reflective material, along with cystoid spaces in the INL of the foveal walls (3 months). Subsequently, the central cavity enlarged and contained hyporeflective fluid (5 months). After resolution of the central cystoid cavity (6.5 months), it developed again (30.5 months). This was associated with the formation of cystoid spaces in the HFL and INL which contained hyporeflective fluid in the parafovea and hyperreflective material in the perifovea.

Figure 3I shows a scan recorded in an eye with central serous chorioretinopathy which was associated with a dome-shaped detachment of the RPE from Bruch's membrane. Large hyperreflective deposits were present in the HFL and ONL of the

fovea and parafovea. There were broad defects of the ELM, EZ, and IZ lines. In addition, there was a gap in the detached RPE layer.

Discussion

The presence of hyperreflective material in the neurosensory retina, which is visible on SD-OCT images as foci, dots, or patches, is a characteristic of different retinal diseases. In the present study, we show that hyperreflective material in the outer macula may exhibit a curved shape, forming thin lines or broad bands between the OPL and ELM. In AMD eyes, such CHRS were referred to as a plume [21]. We describe that CHRS can also be observed on SD-OCT images of eyes with various other diseases without edema, suggesting that it is a more general phenomenon.

CHRS follow the spatial arrangement of the Henle fibers in the HFL and the curved rows of the photoreceptor cell bodies in the ONL (Figure 4A and 4B). This suggests that the hyperreflective material is deposited in the extracellular space between these cellular elements. The dependence of the horizontal extension of CHRS from the distance to the foveal center (Figure 1Ba) is similar to the horizontal extension of Henle fibers which also peaks around 300 µm from the foveal center [38]. This value corresponds with the thickness of the HFL in SD-OCT images (Figure 1C). The average peak length of Henle fibers was described being about 550 µm [39]; the peak horizontal extension of CHRS of up to 500 µm (Figure 1Ba) is similar to this value. We found that the smallest horizontal extension of CHRS was about 150 µm (Figure 1Ba). This corresponds with the horizontal extension of the foveola which has an average diameter of 350 µm [40] and does not contain an OPL [38]. The data suggest that during the formation of CHRS, the deposition of hyperreflective material is directed and restricted by the cellular elements in the outer neuroretina. Another example for a cell-dependent deposition of hyperreflective material is shown in Figure 2I in which the material is restricted to the Müller cell cone.

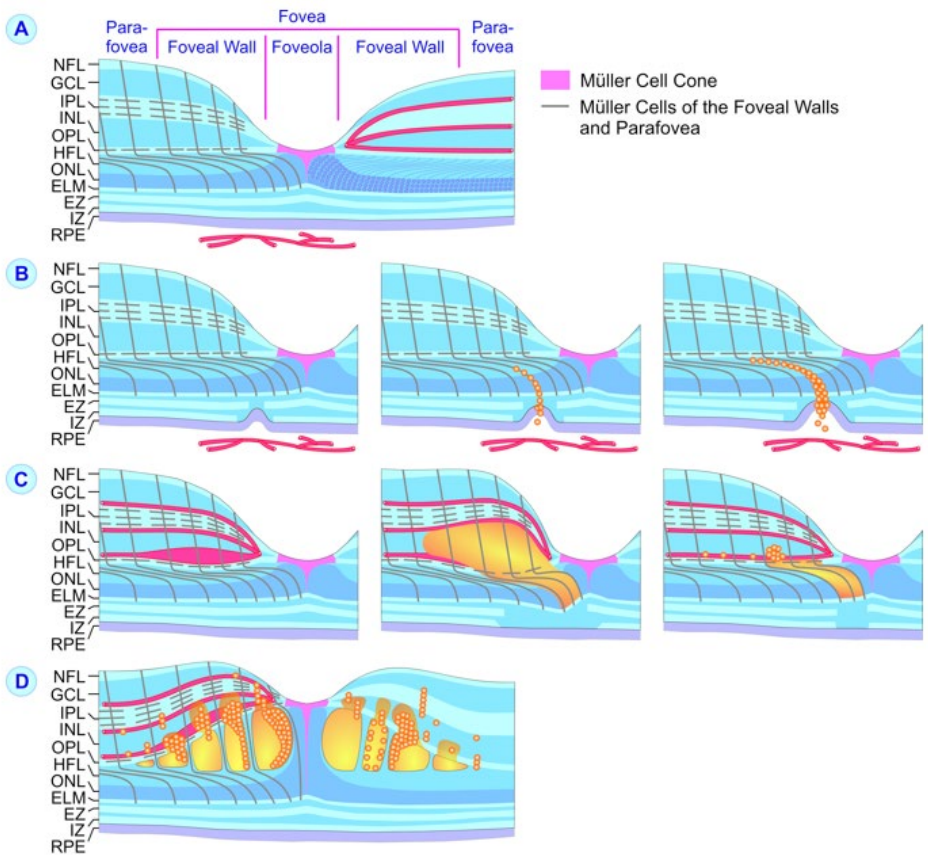

Figure 4: Hypothetical mechanisms of the formation of Curved Hyperreflective Structures (CHRS) in the outer fovea. **A**. Normal fovea. The Müller cell cone in the foveola is shown in pink. Grey lines indicate the main and side processes of the z-shaped Müller cells of the foveal walls and parafovea. The spatial arrangement of the Henle fibers in the Henle Fiber Layer (HFL) and the curved rows of

the photoreceptor cell bodies in the Outer Nuclear Layer (ONL) is stabilized by the outer processes of these cells which also constitute (together with photoreceptor cells) the External Limiting Membrane (ELM). **B**. Possible mechanism of the formation of thin CHRS in response to a local photoreceptor defect. A druse or drusenoid detachment of the Retinal Pigment Epithelium (RPE) causes damage to photoreceptors. Scattered RPE cells migrate into the neuroretina toward the Outer Plexiform Layer (OPL) leaving gaps in the RPE layer which allow a flux of lipoprotein from choroidal vessels. Macrophages, which phagocytoze serum- and photoreceptor-derived lipoprotein, may migrate through the gaps in the RPE layer. **C.** Broad CHRS are formed by vasodilation associated with hemorrhage from the vessels in the inner foveal layers (especially the venules of the deep capillary plexus) due to a sudden increase of the venous pressure. The hemorrhage results in a thickening of the foveal tissue and causes a pressure onto the outer neuroretina, as indicated by the outward deflection of the ELM. Broad CHRS are likely composed of serum-derived lipoprotein and lipid-laden monocytes/macrophages, as well as activated microglia which migrate from the inner to the outer retina. Photoreceptor layer defects occur during or after the formation of broad CHRS suggesting that activated microglial cells cause photoreceptor cell degeneration. **D**. Possible formation of intraretinal hyperreflective deposits in eyes with cystoid macular edema. In patients with elevated local or systemic venous pressure, dilation and leakage of the vessels of the deep capillary plexus leads to exudation of fluid which predominantly accumulates in cystoid spaces in the inner part or the whole thickness of the HFL. Enlargement of the cystoid spaces causes an elevation of the inner foveal layers (Nerve Fiber Layer [NFL] to OPL) and thus a thickening of the foveal tissue; this may be associated with an anterior stretching and thickening of the foveola. Bundles of erected Henle fibers pass through the cystoid spaces. Macrophages or activated microglia that have engulfed lipoprotein migrate through the retina and accumulate within the cystoid spaces. In certain eyes, migrating RPE cells may contribute to the formation of hyperreflective patches in the HFL. EZ: Ellipsoid Zone; GCL: Ganglion Cell Layer; INL: Inner Nuclear Layer; IPL: Inner Plexiform Layer; IZ: Interdigitation Zone.

We found two basic morphologies of CHRS, thin and broad CHRS. Thin CHRS were present in eyes with outer retinal defects resulting from dry AMD (images 1-8 of Figure 1A; Figure 2E), CNV (Figure 2A), chorioretinitis (image 9 of Figure 1A), and AOFVD (Figure 2C). Thin CHRS were also found in eyes which suffered from ocular ischemia (Figure 2B), AION (images 11 and 12 of Figure 1A), PDR (image 13 of Figure 1A), macular scarring (image 10 of Figure 1A), and glaucoma (images 14 and 15 of Figure 1A). Broad CHRS were found in eyes with hemorrhage in the inner foveal layers (Figure 2F-2H). The different morphologies and the diverse retinal diseases of eyes with thin or broad CHRS may suggest distinct mechanisms of pathogenesis.

CHRS were associated with a focal loss of photoreceptor integrity, as indicated by irregular reflectivity, deformation, and/or disruption of EZ and IZ lines. Photoreceptor layer defects were observed to be present before the formation of thin CHRS (Figure 2A, C) and during (Figure 2H) or after the formation of broad CHRS (Figure 2F). The latter may suggest that broad CHRS initiate the deconstruction of photoreceptor segments. In the eye of Figure 2H, hemorrhage in the inner foveal layers was associated with a pressure onto the outer neuroretina and deconstruction of photoreceptor segments. However, the photoreceptor-free area below the CHRS at the end of the examination period was smaller than the EZ- and IZ-free area one month after the first visit. This may suggest that the long-lasting deconstruction of photoreceptor segments is induced by CHRS and not by the pressure onto the outer neuroretina. We found that the BCVA of eyes with CHRS in the foveola varied considerably (Figure 1Bb). This variation cannot be explained with the site and size of the photoreceptor layer defect associated with CHRS. Further factors like the size of drusen or drusenoid RPE detachments in the foveola also influence BCVA which may explain the high variation.

CHRS were only found in eyes without retinal edema. This was even observed in individual eyes. The scans of the eye with hemorrhage of the inner foveal vessels shown in Figure 2G display broad CHRS in the more superior fovea, which did not contain cystoid cavities, while the more inferior fovea contained such cavities, but not CHRS. In the eye with CNV associated with a serous detachment of the fovea shown in Figure 2A, CHRS was formed after resolution of the subretinal edema.

It is unclear why the deposition of hyperreflective material in the outer neuroretina follows the cellular arrangement in some eyes (e.g., Figure 2C, left side of Figure 2E), but not in other eyes (e.g., Figure 2D, right side of Figure 2E). In eyes with edema, CHRS may not be formed because extracellular accumulation of excess fluid alters the spatial arrangement of the fibers and cells in the outer retina. Further causes may be possible. For example, differences in the hydrostatic pressure between the blood in the choroidal vessels and the neuroretina may push blood-derived material and RPE cells into the outer neuroretina which disrupts the cellular structure of the tissue.

The pathogenesis of CHRS is currently unclear. In dependence to the morphology of CHRS and the type of retinal disease, there are various potential etiologies.

1. CHRS may represent lipoprotein exudates. Breaks in the RPE layer may allow lipoprotein extravasation from the choroidal vessels; the intraretinal spread is restrained by the OPL, which is a fluid conductivity barrier [41], resulting in deposition of extravasated lipoprotein in the ONL and HFL (Figure 3I). Leakage of vessels in the inner foveal layers may give rise to exudation of

lipoproteins which participates in the formation of broad CHRS (Figure 2F-2H). The expulsion of hyperreflective material into the outer neuroretina through breaks in the RPE layer may be supported by high blood pressure. In patients with diabetic retinopathy, elevated serum lipid levels were described to be associated with an increased risk of intraretinal deposition of hyperreflective material (hard exudate) [2,26,30,42-44]; this suggests that the intraretinal hyperreflective material is (at least in part) derived from serum lipoproteins.

2. CHRS may be formed by migrating RPE cells. It was suggested that the hyperreflective structures in the outer neuroretina of AMD eyes are formed by RPE cells which migrated towards the inner retina; the migration of the cells may leave gaps in the RPE layer [6,8,9,17,21,45,46,]. It was shown that hyperreflective foci in all retinal layers of AMD eyes including such which surround capillaries in the inner foveal layers are formed by migrating RPE cells [6,21]. Intraretinal hyperreflective foci associated with acquired vitelliform lesions were supposed to be migrating RPE cells which contain highly reflective melanosomes, lipofuscin, and melanolipofuscin granules [5]. The assumption that thin CHRS are formed by migrating RPE cells is supported by various findings: In areas of drusen or drusenoid RPE detachments, CHRS were connected to the RPE (images 3, 6, 7, 9 of Figure 1A; Figure 2E); in various eyes, CHRS did not reach the OPL (images 5, 10, 11, 15 of Figure 1A), suggesting that it might be formed by an anterior growth from the ELM; in one eye, CHRS was apparently formed from irregularly shaped hyperreflective material which lay near the ELM and which grew time-dependently towards the OPL (Figure 2A). Thin hyperreflective lines were composed of separated dots (images 2, 5, 14 of Figure 1A), which may represent single RPE cells which lay in line, while broader lines were composed of adjoining dots (e.g., images 1 and 15 of Figure 1A) which may represent grouped RPE cells. On the other hand, there were no morphological alterations of the RPE in eyes with broad CHRS (Figure 2F-2H), suggesting that RPE cell migration did not contribute to the formation of these structures.

3. CHRS may represent migrating lipoprotein-laden phagocytes, i.e., infiltrating monocytes/macrophages and/or activated microglial cells. At least parts of hyperreflective foci in the retina of diabetic patients are supposed to represent phagocytes like macrophages or activated microglia that have engulfed lipoprotein [28-33]. In wet AMD, hyperreflective dots, which scatter through the retina and accumulate in cystoid spaces in outer retinal layers, were suggested to be formed by microglia [15]. Activated microglia migrate from the inner to the outer retina and phagocytize cell debris [47]. Microglia migration may be triggered by photoreceptor deconstruction because photoreceptor proteins are potent immunogens [48,49]. Phagocytotic monocytes/macrophages and microglia contribute to photoreceptor cell degeneration by the release of cytotoxic cytokines [50-52]. Microglial cells containing photoreceptor debris exit the retina via retinal and choroidal vessels, reach the spleen, and act as antigen-presenting cells [53,54].

We found in various eyes that CHRS in the outer macula were composed of hyperreflective dots (Figure 1A); the mean dot diameter was 31 µm. This value is similar to the diameter of hyperreflective foci in the retina of eyes with DME (approximately 30 µm [2]. Hyperreflective dots in the macula of eyes with retinal vascular diseases have a diameter of about 27 µm [32], and macrophages have a diameter of about 21 µm [55]. CHRS in the outer macula may be formed by activated microglial cells, which show cell body enlargement [47], and/or macrophages which are enlarged after phagocytosis of lipoprotein derived from the blood or degenerated photoreceptors, and which migrate from defects in the RPE or the capillaries in the INL into the outer neuroretina. The right side of Figure 2E shows the presence of a hyperreflective patch in the INL after partial regression of hyperreflective material in the HFL. It could be that it is caused by lipoprotein-laden microglia which leave the retina via the vessels in the INL.

Thin CHRS are often thicker at the ELM and thinner in the HFL, and may not reach the OPL (images 5, 10, 11, 15 of Figure 1A). In addition, photoreceptor layer defects were observed in two eyes before the formation of thin CHRS (Figure 2A, C). These findings may suggest that thin CHRS evolve in response to a local photoreceptor defect by infiltration of macrophages or RPE cells into the outer neuroretina (Figure 4B). Broad CHRS are thicker in the HFL and thinner at the ELM, and photoreceptor layer defects occur during or after the formation of broad CHRS (Figure 2F, H). These findings may suggest that broad CHRS are composed of activated microglia, which migrate from the inner to the outer retina, and monocytes/macrophages which enter the retinal parenchyme from the vessels in the inner foveal layers (Figure 4C). The finding that photoreceptor layer defects may occur during or after the formation of broad CHRS (Figure 2F, H) is in agreement with previous studies which showed that activated microglial cells cause photoreceptor cell degeneration [50-52].

There are further possibilities which may explain the nature of CHRS. It could be that in eyes with retinal hemorrhages, accumulation of heme contributes to the formation of broad CHRS. The formation of thin CHRS may also reflect the translocation of lipofuscin granules and mitochondria in photoreceptor cells [56,57]. In addition, reactive Müller cell processes may contribute to the formation of thin CHRS. Focal photoreceptor damage and migrating phagocytes and RPE cells may induce gliosis associated with a thickening of the outer Müller cell processes which draw through the HFL and ONL from the OPL and ELM (Figure 4A) [38]. It was shown that hyperreflective dots in the inner layer of the foveola are caused by light reflections at optically dense structures of Müller cells [58] which are likely formed by upregulated intermediate filaments. Increased intermediate filament expression,

which is a characteristic of Müller cell gliosis [59], correlates with a higher stiffness of Müller cells [60] which will increase the capacity of the cells to resist tractional forces and to guarantee the structural stability of the tissue. In addition, Müller cells are known to phagocytize serum-derived material [47]. Therefore, CHRS could also represent thickened Müller cell processes which contain phagocytozed lipoprotein that flowed through RPE gaps into the neuroretina. Further investigations are needed to determine the pathogenesis of CHRS.

The retina of eyes with CME contained hyperreflective foci and cystoid spaces with hypo- (Figure 3D, G, H) or medium-reflective fluid (Figure 3E, F) and deposits of hyperreflective material (Figure 3C-3H). Hyporeflective cystoid spaces likely contain extracellular fluid. Medium-reflective fluid may contain exudate of serum lipoprotein dissolved in extracellular fluid while the hyperreflective material may be formed by accumulation of extravasated lipoprotein and/or lipoprotein-laden phagocytes. Edematous cystoid spaces are preferentially localized in the HFL of the foveal walls, para-, and perifovea (Figsure 3C-3H and 4D) and in the foveola (Figure 3F-3H); in one eye, cystoid spaces were also present in the INL (Figure 3H). Hyperreflective material in the HFL may form a stellate figure of hard exudates in the macula according to the spatial arrangement of Henle fibers (Figure 3E) [61,62]. Hyperreflective material may disappear within weeks (Figure 2F) or months (Figure 3B).

In eyes without (Figure 3A, B) and with CME (Figure 3C-3G), the largest amount of hyperreflective material is found in the HFL (Figure 4D) [22-25]. Hyperreflective material may form continuous structures which extend from the INL to the HFL (Figure 3A-3H), suggesting that the main source of the material in the HFL are leaky vessels in the INL. In the eye of Figure 3B, lipoprotein exudation from the choroidea or RPE cell migration toward the neuroretina may contribute to the hyperreflective material in the HFL, as indicated by the continuities between the materials in the HFL and subretinal space. In various eyes, the hyperreflective material in the INL, OPL, and HFL was composed of adjoining dots (Figure 3B, F), suggesting that parts of the hyperreflective patches represent aggregated phagocytes. In eyes with outer retinal disorders, hyperreflective material in the HFL may be derived from leakage of RPE (Figure 3I).

The preferential deposition of hyperreflective material in the HFL was suggested to result from vasodilation associated with leakage or hemorrhage from the vessels of the deep capillary plexus in patients with increased local or systemic venous pressure [2,26,37]. The deep capillary plexus provides the main venous outflow from the retinal vessels and is at the greatest risk of bleeding due to a sudden rise of the venous pressure [63,64]. The preferential deposition of the hyperreflective material and the formation of edematous cystoid spaces in the HFL is supported by the histological feature of this layer. The HFL is a layer with a low mechanical cohesion because it is composed of Henle fibers which are not connected and which can be shifted or even erected, e.g., in eyes with anterior traction to the retina or intraretinal fluid accumulation resulting in foveoschisis or edematous cystoid spaces [65,66]. Erection of Henle fibers results in a large increase of the extracellular space volume in the HFL which can serve as a depot for high amounts of excess fluid, blood-derived lipoprotein, and phagocytes.

Conclusion

CHRS may be present in eyes with different retinal disorders without edema. CHRS form thin curved lines or broad bands in the HFL and ONL of the macula which follow the spatial arrangement of Henle fibers and the rows of photoreceptor cell bodies. In eyes with AMD, thin CHRS may be associated with drusen or drusenoid RPE detachments. The formation of broad CHRS is caused by hemorrhages in the inner foveal layers. CHRS are associated with a focal loss of photoreceptor integrity which is present before the formation of thin CHRS and during or after the formation of broad CHRS. The retina of eyes with CME may contain hyperreflective foci and cystoid spaces which comprise hypo- or medium-reflective fluid and hyperreflective material, but not CHRS.

References

1. Kon Y, Iida T, Maruko I, Saito M (2008) The optical coherence tomography-ophthalmoscope for examination of central serous chorioretinopathy with precipitates. Retina 28: 864-869.
2. Bolz M, Schmidt-Erfurth U, Deak G, Mylonas G, Kriechbaum K, et al. (2009) Optical coherence tomographic hyperreflective foci: A morphologic sign of lipid extravasation in diabetic macular edema. Ophthalmology 116: 914-920.
3. Ogino K, Murakami T, Tsujikawa A, Miyamoto K, Sakamoto A, et al. (2012) Characteristics of optical coherence tomographic hyperreflective foci in retinal vein occlusion. Retina 32: 77-85.
4. Coscas G, De Benedetto U, Coscas F, Li Calzi CI, Vismara S, et al. (2013) Hyperreflective dots: A new spectral-domain optical coherence tomography entity for follow-up and prognosis in exudative age-related macular degeneration. Ophthalmologica 229: 32-37.
5. Chen KC, Jung JJ, Curcio CA, Balaratnasingam C, Gallego-Pinazo R, et al. (2016) Intraretinal hyperreflective foci in acquired vitelliform lesions of the macula: Clinical and histologic study. Am J Ophthalmol 164: 89-98.
6. Curcio CA, Zanzottera EC, Ach T, Balaratnasingam C, Freund KB (2017) Activated retinal pigment epithelium, an optical coherence tomography biomarker for progression in age-related macular degeneration. Invest Ophthalmol Vis Sci 58: BIO211-BIO226.
7. Berasategui B, Fonollosa A, Artaraz J, Ruiz-Arruza I, Ríos J, et al. (2018) Behavior of hyperreflective foci in non-infectious uveitic macular edema, a 12-month follow-up prospective study. BMC Ophthalmology 18: 179.
8. Christenbury JG, Folgar FA, O'Connell RV, Chiu SJ, Farsiu S, et al. (2013) Progression of intermediate age-related macular degeneration with proliferation and inner retinal migration of hyperreflective foci. Ophthalmology 120: 1038-1045.

9. Lei J, Balasubramanian S, Abdelfattah NS, Nittala MG, Sadda SR (2017) Proposal of a simple optical coherence tomography-based scoring system for progression of age-related macular degeneration. Graefes Arch Clin Exp Ophthalmol 255: 1551-1558.

10. Nassisi M, Fan W, Shi Y, Lei J, Borrelli E, et al. (2018) Quantity of intraretinal hyperreflective foci in patients with intermediate age-related macular degeneration correlates with 1-year progression. Invest Ophthalmol Vis Sci 59: 3431-3439.

11. Kang JW, Chung H, Kim HC (2016) Correlation of optical coherence tomographic hyperreflective foci with visual outcomes in different patterns of diabetic macular edema. Retina 36: 1630-1639.

12. Lee H, Lee J, Chung H, Kim HC (2016) Baseline spectral domain optical coherence tomographic hyperreflective foci as a predictor of visual outcome and recurrence for central serous chorioretinopathy. Retina 36: 1372-1380.

13. Matet A, Daruich A, Zola M, Behar-Cohen F (2018) Risk factors for recurrences of central serous chorioretinopathy. Retina 38: 1403-1414.

14. Srinivas S, Nittala MG, Hariri A, Pfau M, Gasperini J, et al. (2018) Quantification of intraretinal hard exudates in eyes with diabetic retinopathy by optical coherence tomography. Retina 38: 231-236.

15. Coscas G, De Benedetto U, Coscas F, Li Calzi CI, Vismara S, et al. (2013) Hyperreflective dots: A new spectral-domain optical coherence tomography entity for follow-up and prognosis in exudative age-related macular degeneration. Ophthalmologica 229: 32-37.

16. Schuman SG, Koreishi AF, Farsiu S, Jung Sh, Izatt JA, et al. (2009) Photoreceptor layer thinning over drusen in eyes with age-related macular degeneration imaged in vivo with spectral-domain optical coherence tomography. Ophthalmology 116: 488-496.e2.

17. Ho J, Witkin AJ, Liu J, Chen Y, Fujimoto JG, et al. (2011) Documentation of intraretinal retinal pigment epithelium migration via high-speed ultrahigh-resolution optical coherence tomography. Ophthalmology 118: 687-693.

18. Folgar FA, Chow JH, Farsiu S, Wong WT, Schuman SG, et al. (2012) Spatial correlation between hyperpigmentary changes on color fundus photography and hyperreflective foci on SDOCT in intermediate AMD. Invest Ophthalmol Vis Sci 53: 4626-4633.

19. Ouyang Y, Heussen FM, Hariri A, Keane PA, Sadda SR (2013) Optical coherence tomography-based observation of the natural history of drusenoid lesion in eyes with dry age-related macular degeneration. Ophthalmology 120: 2656-2665.

20. Leuschen JN, Schuman SG, Winter KP, McCall MN, Wong WT, et al. (2013) Spectral-domain optical coherence tomography characteristics of intermediate age-related macular degeneration. Ophthalmology 120: 140-150.

21. Balaratnasingam C, Messinger JD, Sloan KR, Yannuzzi LA, Freund KB, et al. (2017) Histologic and optical coherence tomographic correlates in drusenoid pigment epithelium detachment in age-related macular degeneration. Ophthalmology 124: 644-656.

22. Yanoff M (1969) Ocular pathology of diabetes mellitus. Am J Ophthalmol 67: 21-38.

23. Murata T, Ishibashi T, Inomata H (1992) Immunohistochemical detection of extravasated fibrinogen (fibrin) in human diabetic retina. Graefes Arch Clin Exp Ophthalmol 230: 428-431.

24. Takagi H, Otani A, Kiryu J, Ogura Y (1999) New surgical approach for removing massive foveal hard exudates in diabetic macular edema. Ophthalmology 106: 249-256.

25. Otani T, Kishi S (2001) Tomographic findings of foveal hard exudates in diabetic macular edema. Am J Ophthalmol 131: 50-54.

26. Davoudi S, Papavasileiou E, Roohipoor R, Cho H, Kudrimoti S, et al. (2016) Optical coherence tomography characteristics of macular edema and hard exudates and their association with lipid serum levels in type 2 diabetes. Retina 36: 1622-1629.

27. Uji A, Murakami T, Nishijima K, Akagi T, Horii T, et al. (2012) Association between hyperreflective foci in the outer retina, status of photoreceptor layer, and visual acuity in diabetic macular edema. Am J Ophthalmol 153: 710-717.e1.

28. Wolter JR, Goldsmith RI, Phillips RL (1957) Histopathology of the starfigure of the macular area in diabetic and angiospastic retinopathy. AMA Arch Ophthalmol 57: 376-385.

29. Toussaint D, Cogan DG, Kuwabara T (1962) Extravascular lesions of diabetic retinopathy. Arch Ophthalmol 67: 42-47.

30. Cusick M, Chew EY, Chan C-C, Kruth HS, Murphy RP, et al. (2003) Histopathology and regression of retinal hard exudates in diabetic retinopathy after reduction of elevated serum lipid levels. Ophthalmology 110: 2126-2133.

31. Vujosevic S, Bini S, Midena G, Berton M, Pilotto E, et al. (2013) Hyperreflective intraretinal spots in diabetics without and with nonproliferative diabetic retinopathy: An *in vivo* study using spectral domain OCT. J Diabetes Res 2013: 491835.

32. Yamaguchi M, Nakao S, Kaizu Y, Kobayashi Y, Nakama et al. (2016) High-resolution imaging by adaptive optics scanning laser ophthalmoscopy reveals two morphologically distinct types of retinal hard exudates. Sci Rep 6: 33574.

33. Lee H, Jang H, Choi YA, Kim HC, Chung H (2018) Association between soluble CD14 in the aqueous humor and hyperreflective foci on optical coherence tomography in patients with diabetic macular edema. Invest Ophthalmol Vis Sci 59: 715-721.

34. Lujan BJ, Roorda A, Knighton RW, Carroll J (2011) Revealing Henle's fiber layer using spectral domain optical coherence tomography. Invest Ophthalmol Vis Sci 52: 1486-1492.

35. Otani T, Yamaguchi Y, Kishi S (2011) Improved visualization of Henle fiber layer by changing the measurement beam angle on optical coherence tomography. Retina 31: 497-501.

36. Syrbe S, Kuhrt H, Gärtner U, Habermann G, Wiedemann P, et al. (2018) Müller glial cells of the primate foveola: An electron microscopical study. Exp Eye Res 167: 110-117.

37. Baumal CR, Sarraf D, Bryant T, Gui W, Muakkassa N, et al. (2021) Henle fibre layer haemorrhage: Clinical features and pathogenesis. Br J Ophthalmol 105: 374-380.

38. Bringmann A, Syrbe S, Görner K, Kacza J, Francke M, et al. (2018) The primate fovea: Structure, function and development. Prog Retin Eye Res 66: 49-84.

39. Drasdo N, Millican CL, Katholi CR, Curcio CA (2007) The length of Henle fibers in the human retina and a model of ganglion receptive field density in the visual field. Vision Res 47: 2901-2911.

40. Curcio CA, Sloan KR, Kalina RE, Hendrickson AE (1990) Human photoreceptor topography. J Comp Neurol 292: 497-523.

41. Antcliff RJ, Hussain AA, Marshall J (2001) Hydraulic conductivity of fixed retinal tissue after sequential excimer laser ablation: Barriers limiting fluid distribution and implications for cystoid macular edema. Arch Ophthalmol 119: 539-544.

42. Klein BE, Moss SE, Klein R, Surawicz TS (1991) The Wisconsin Epidemiologic Study of Diabetic Retinopathy. XIII. Relationship of serum cholesterol to retinopathy and hard exudate. Ophthalmology 98: 1261-1265.

43. Chew EY, Klein ML, Ferris FL 3rd, Remaley NA, Murphy RP, et al. (1996) Association of elevated serum lipid levels with retinal hard exudate in diabetic retinopathy. Early Treatment Diabetic Retinopathy Study (ETDRS) Report 22. Arch Ophthalmol 114: 1079-1084.

44. Sasaki M, Kawasaki R, Noonan JE, Wong TY, Lamoureux E, et al. (2013) Quantitative measurement of hard exudates in patients with diabetes and their associations with serum lipid levels. Invest Ophthalmol Vis Sci 54: 5544-5550.

45. Pieroni CG, Witkin AJ, Ko TH, Fujimoto JG, Chan A, et al. (2006) Ultrahigh resolution optical coherence tomography in non-exudative age related macular degeneration. Br J Ophthalmol 90: 191-197.

46. Fleckenstein M, Charbel Issa P, Helb HM, Schmitz-Valckenberg S, Finger RP, et al. (2008) High-resolution spectral domain-OCT imaging in geographic atrophy associated with age-related macular degeneration. Invest Ophthalmol Vis Sci 49: 4137-4144.

47. Reichenbach A, Bringmann A (2015) Retinal Glia. In: Verkhratsky A, Parpura V (Eds.) Colloquium Series on Neuroglia in Biology and Medicine: From Physiology to Disease. Morgan & Claypool Life Sciences, Philadelphia, PA. 2: 1-644.

48. Rahi AH, Addison DJ (1983) Autoimmunity and the outer retina. Trans Ophthalmol Soc U K 103: 428-437.

49. Gupta N, Brown KE, Milam AH (2003) Activated microglia in human retinitis pigmentosa, late-onset retinal degeneration, and age-related macular degeneration. Exp Eye Res 76: 463-471.

50. Langmann T (2007) Microglia activation in retinal degeneration. J Leukoc Biol 81: 1345-1351.

51. Nakazawa T, Hisatomi T, Nakazawa C, Noda K, Maruyama K, et al. (2007) Monocyte chemoattractant protein 1 mediates retinal detachment-induced photoreceptor apoptosis. Proc Natl Acad Sci U S A 104: 2425-2430.

52. Wang NK, Lai CC, Liu CH, Yeh LK, Chou CL, et al. (2013) Origin of fundus hyperautofluorescent spots and their role in retinal degeneration in a mouse model of Goldmann-Favre syndrome. Dis Model Mech 6: 1113-1122.

53. Raoul W, Keller N, Rodéro M, Behar-Cohen F, Sennlaub F, et al. (2008) Role of the chemokine receptor CX3CR1 in the mobilization of phagocytic retinal microglial cells. J Neuroimmunol 198: 56-61.

54. Joly S, Francke M, Ulbricht E, Beck S, Seeliger M, et al. (2009) Cooperative phagocytes: resident microglia and bone marrow immigrants remove dead photoreceptors in retinal lesions. Am J Pathol 174: 2310-2323.

55. Krombach F, Münzing S, Allmeling AM, Gerlach JT, Behr J, et al. (1997) Cell size of alveolar macrophages: An interspecies comparison. Environ Health Perspect 105: 1261-1263.

56. Litts KM, Messinger JD, Freund KB, Zhang Y, Curcio CA (2015) Inner segment remodeling and mitochondrial translocation in cone photoreceptors in age-related macular degeneration with outer retinal tubulation. Invest Ophthalmol Vis Sci 56: 2243-2253.

57. Echols BS, Clark ME, Swain TA, Chen L, Kar D, et al. (2020) Hyperreflective foci and specks are associated with delayed rod-mediated dark adaptation in nonneovascular age-related macular degeneration. Ophthalmol Retina 4: 1059-1068.

58. Yokotsuka K, Kishi S, Shimizu K (1997) White dot fovea. Am J Ophthalmol 123: 76-83.

59. Bringmann A, Iandiev I, Pannicke T, Wurm A, Hollborn M, et al. (2009) Cellular signaling and factors involved in Müller cell gliosis: Neuroprotective and detrimental effects. Prog Retin Eye Res 28: 423-451.

60. Lu YB, Iandiev I, Hollborn M, Körber N, Ulbricht E, et al. (2011) Reactive glial cells: Increased stiffness correlates with increased intermediate filament expression. FASEB J 25: 624-631.

61. Bedell AJ (1953) The stellate figure in the macular region. Trans Am Ophthalmol Soc 51: 257-272.

62. Makino S, Watanabe M, Tampo H (2014) Stellate figure in the macula: Visualization in the Henle fiber layer on optical coherence tomography. Clin Optometry 6: 1-3.

63. Adhi M, Filho MAB, Louzada RN, Kuehlewein L, de Carlo TE, et al. (2016) Retinal capillary network and foveal avascular zone in eyes with vein occlusion and fellow eyes analyzed with optical coherence tomography angiography. Invest Ophthalmol Vis Sci 57: OCT486-OCT494.

64. Freund KB, Sarraf D, Leong BCS, Garrity ST, Vupparaboina KK, et al. (2018) Association of optical coherence tomography angiography of collaterals in retinal vein occlusion with major venous outflow through the deep vascular complex. JAMA Ophthalmol 136: 1262-1270.

65. Bringmann A, Reichenbach A, Wiedemann P (2004) Pathomechanisms of cystoid macular edema. Ophthalmic Res 36: 241-249.

66. Govetto A, Hubschman J-P, Sarraf D, Figueroa MS, Bottoni F, et al. (2020) The role of Müller cells in tractional macular disorders: An optical coherence tomography study and physical model of mechanical force transmission. Br J Ophthalmol 104: 466-472.